Charged Particle Imaging of the Deprotonated Octatrienoic Acid Anion: Evidence for a Photo-induced Cyclization Reaction

Christopher W. West,[a] James N. Bull[b] and Jan R. R. Verlet[c,]*

[a]Department of Chemistry, Graduate School of Science, Kyoto University, Kitashirakawa

*Oiwake-cho, Sakyo-Ku, Kyoto 606-8502, Japan*

[b]School of Chemistry, University of Melbourne, Parkville, Melbourne, VIC 3010, Australia

[c]Department of Chemistry, University of Durham, Durham DH1 3LE, United Kingdom

*Email: j.r.r.verlet@durham.ac.uk

Abstract

The photoelectron spectroscopy of the deprotonated octatrienoic acid anion, $[C_7H_9–CO_2]^-$, shows the formation of $[C_7H_9]^-$ and loss of H^- at $hv = 4.13$ eV. Using velocity map imaging, the H^- fragment was characterized to have a Boltzmann-like kinetic energy distribution consistent with dissociation on a ground electronic state. Similar dynamics were not observed at $hv = 4.66$ eV even though there is clear evidence for recovery of the ground electronic state of $[C_7H_9–CO_2]^-$. In accord with supporting electronic structure calculations, the production of H^- at $hv = 4.13$ eV is explained by an excited state dissociation of CO_2 to form $[C_7H_9]^-$, which subsequently undergoes a ring-closure isomerization reaction to yield toluene and H^-. These data represent the first-evidence for a photo-induced ring-closing isomerization reaction in an anionic polyene and provides an interesting example of the rich anion dynamics that can occur in the detachment continuum and that can influence photochemistry.
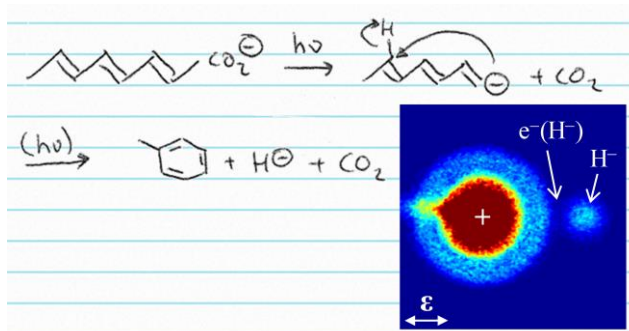
TOC graphic

Polyenes such as retinal, carotene, and antimycotic agents are common natural pigments due to their extended π-electron systems that enable visible light to induce bright π-π* transitions.[1-5] In many cases, these transitions lead to structural changes as the π* excited state character promotes rotation about the polyene backbone. The best-known example is the retinal protonated Schiff base, which undergoes photoisomerization within the opsin protein and initiates the first step in the visual phototransduction cycle.[6-8] The retinal protonated Schiff base chromophore can undergo many photoisomerization and thermal reversion cycles in the protein; however, as an isolated cation, it may degrade through an intramolecular cyclization.[9-12] Similar isomerization processes are also known to occur in isolated polyene anions, for example, following collisional-activation.[13] However, direct photo-induced isomerization studies on anionic polyenes have not been studied, in part because direct photodetachment (i.e. instantaneous light-induced electron ejection) is an open channel and one might anticipate that the electron will simply leave. But, it is also well-established that π* resonances can often complicate the photoelectron spectroscopy of bright chromophore anions, particularly in polyaromatic and highly conjugated systems, where photoexcitation to resonances can be much more probable than direct photodetachment.[14-17] The dynamics of such resonances can have striking effects on the measured photoelectron spectra, since ultrafast excited state nuclear motion can compete with autodetachment.[18,19] These effects can take the form of changing Franck-Condon factors, internal conversion dynamics, or dissociation dynamics leading to an anionic fragment from which an electron is subsequently photodetached. Several recent photoelectron studies on conjugated anions have shown that photoexcitation of resonances followed by ground electronic state recovery is a very efficient process.[15,20] Alternatively, dissociation can occur directly on the potential energy surface of the resonance if it is repulsive,[21] or from the ground electronic state provided there is an efficient internal conversion route and the total vibrational energy exceeds the bond

dissociation energy.[22] In the latter case, the dissociation products can provide insight into the ground state chemical transformations. Because ground-state isomerization reactions can occur in polyene anions and because internal conversion can compete with autodetachment, one might also expect polyene anions to undergo cyclization reactions following photo-excitation.

In the present photoelectron imaging study, we show that UV excitation ($hv = 4.13$ eV) of the deprotonated polyeneoic acid anion, octatrienoic acid, $[C_7H_9–CO_2]^-$, leads to the formation of both $[C_7H_9]^-$ and the hydride anion, H^-. We adapt the photoelectron velocity-mapping conditions to allow direct imaging of H^-, which exhibits a Boltzmann-like kinetic energy release distribution. Combining all experimental evidence with supporting electronic structure calculations, we propose a two-step mechanism. Firstly, photoexcitation of a resonance at $hv = 4.13$ eV leads to excited state dissociation of CO_2 to produce ground electronic state $[C_7H_9]^-$. Next, the vibrationally-hot $[C_7H_9]^-$ undergoes an intramolecular cyclization to form toluene and H^-. Our results demonstrate that anion resonances can lead to rich photochemistry and that the combination of photoelectron imaging and charged-particle imaging is a useful tool for probing the intermediates and products of unimolecular anion reactions.

Experimentally, $[C_7H_9–CO_2]^-$ (Figure 1) was generated by electrospray ionisation, mass-selected and intersected with laser pulses (~5 ns duration) at 4.13 eV (300 nm) or 4.66 eV (266 nm) at the centre of a perpendicular velocity-map imaging (VMI) spectrometer.[23,24] The VMI spectrometer has been optimised to perform photoelectron spectroscopy by gating the imaging detector with ~100 ns gate pulse and reconstructing the raw image.[25] However, the same perpendicular VMI spectrometer can also be used to image other charged species, such as H^-. Supporting ground electronic structure calculations were performed at the G4

4

level of theory and resonance energetics computed at multi-state XCMQDPT2 level of theory.[26,27]

The photoelectron spectra of $[C_7H_9–CO_2]^-$ taken at $hv = 4.13$ eV and 4.66 eV are shown in Figure 1(a) and (b), respectively. The photoelectron spectra are dominated by a peak at low electron kinetic energy, eKE, which is generally indicative of the indirect electron loss process of thermionic emission.[15,20,28,29] In addition to this low eKE peak, there are several minor features at higher eKE. In the $hv = 4.13$ eV spectrum, the low eKE peak has a shoulder that extends up to ~1.4 eV and a weak feature that peaks at eKE ~ 2.5 eV as indicated by the asterisk in Figure 1(a). The photoelectron spectrum at $hv = 4.66$ eV, shown in Figure 1(b), is broadly similar, although the shoulder to the dominating low eKE peak is larger than at $hv = 4.13$ eV and extends to eKE ~1.9 eV, which is consistent with a direct
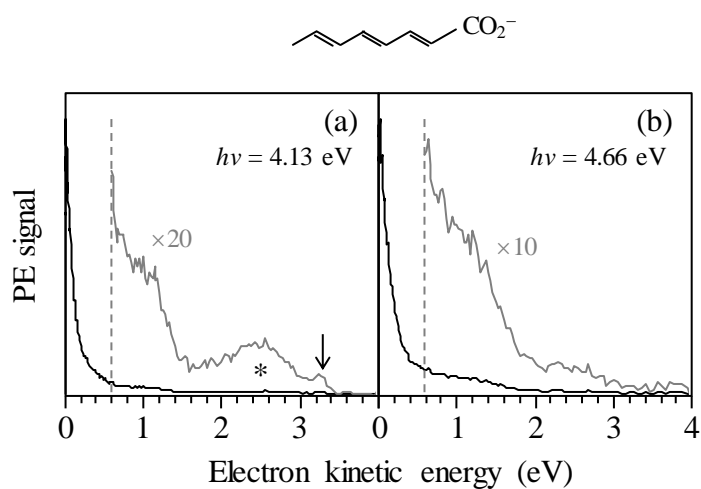

Figure 1: Photoelectron spectra of $[C_7H_9–CO_2]^-$ taken at (a) 300 nm (4.13 eV) and (b) 266 nm (4.66 eV). Signal at eKE > 0.6 eV has been magnified for clarity. The asterisk highlights the peak suspected to result from photodetachment from $[C_7H_9]^-$. The vertical downward arrow identifies the photodetachment from H^-. The structure of $[C_7H_9–CO_2]^-$ is shown.
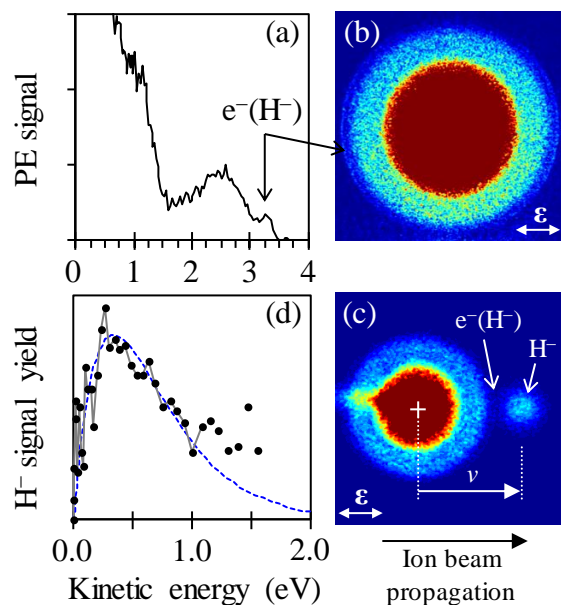
Figure 2: Photoelectron spectra of $[C_7H_9–CO_2]^-$ taken at (a) 300 nm (4.13 eV) that was reconstructed from the raw photoelectron image in (b). In (c), in addition to the photoelectron image, H^- is observed (imaging gate of 1μs) and is offset from the photoelectron feature because of the velocity of the primary ion beam, v. The kinetic energy release distribution associated with the H^- fragment is shown in (d) along with a Boltzmann distribution (dashed line) that serves as a guide to the eye. The polarisation vector, ε, is indicated in (b) and (c).

photodetachment process. The $hv = 4.66$ eV spectrum does not, however, show the clear peak around eKE ~ 2.5 eV (or at eKE ~ 3.0 eV taking into account the additional photon energy).

In addition to the peak at eKE ~ 2.5 eV in the $hv = 4.13$ eV photoelectron spectrum, a discernible peak is present at eKE ~ 3.3 eV, as indicated by the arrow in Figure 1(a). The peak is more clearly seen in the magnified photoelectron spectrum in Figure 2(a) and the raw photoelectron image in Figure 2(b). Unlike the other features at lower eKE that are all isotropic in the photoelectron image, the photoelectron feature corresponding to the peak at eKE ~ 3.3 eV is highly anisotropic (β_2 ~ +2) corresponding to electron ejection parallel to the laser polarisation axis, ε.[30] Furthermore, the peak width is close to the velocity-mapping resolution (~0.17 eV at 3.3 eV), which is surprising considering the molecular size of $[C_7H_9–CO_2]^-$ and that the anions were initially thermalized to 300 K in the ion trap. Sharp

photoelectron features have been observed in anion photoelectron spectra of large molecules, where they have been found to correspond to weakly bound non-valence orbitals such as dipole-bound states.[31] However, *trans*-[C_7H_9–CO_2] has a calculated dipole moment of 1.7 D, which is insufficient to support a dipole-bound state.[32] Moreover, the binding energy (eBE = hv – eKE) is inconsistent with a weakly bound non-valence orbital. In the present case, the narrow peak has a binding energy of ~0.8 eV, which is close to the known electron affinity of H at 0.75497 eV (the electron affinities of C or O are inconsistent with the observed binding energy).[33] In addition, the angular anisotropy associated with this peak suggests the outgoing wave has angular momentum of $l = 1$ (p-wave), which is expected for photodetachment of an electron from the 1s orbital ($l = 0$) of H^-.[30] We therefore assign the narrow feature to result from H^- photodetachment, which must be first dissociated from [C_7H_9–CO_2]$^-$. Therefore, this two-photon detachment process must occur within the duration of the 5 ns laser pulse.

To further characterise the dissociation mechanism we performed velocity-map imaging of the H^- product. Ground state dissociation involves internal vibrational energy redistribution, which occurs on a picosecond timescale, prior to the excess energy being statistically imparted into the relevant modes to induce bond cleavage.[34] If this mechanism is in operation, the kinetic energy release associated with the H^- fragment should exhibit a Boltzmann-like distribution. Additionally, the angular distribution associated with H^- dissociation may be expected to be isotropic, since molecular rotation is much faster than statistical unimolecular dissociation. In contrast, a prompt excited state dissociation may be expected to produce H^- with a high (non-Boltzmann) and potentially an anisotropic kinetic energy release distribution. Such dynamical behaviour is well known for excited state H atom dissociation.[35] Although the present experiment was not designed to characterize ion fragments, our arrangement still allowed the H^- product to be imaged, albeit offset from the

centre along the propagation axis of the ion beam because of the perpendicular VMI arrangement and the mass (time-of-flight) difference between an electron and H^-.

To velocity-map H^-, we extended the imaging acquisition gate on the MCP from 100 ns to 1 μs to account for the much longer time-of-flight of H^- compared with photoelectrons. Figure 2(c) shows a raw photoelectron image of $[C_7H_9–CO_2]^-$ taken at $hv = 4.13$ eV with an MCP gate of 1 μs and a VMI voltage of 1500 V (which is three times that used for photoelectron imaging). The photoelectron image can be identified in Figure 2(c), although is reduced in radial extent due to the higher VMI voltages. The tail-like signal observed to the left of this image arises from delayed photoelectron emission over the 1 μs MCP gate width; after a few 100 ns, the main ion packet has moved out of the interaction region and the VMI condition is no longer maintained leading to a smearing out of the photoelectron signal at the opposite side of the emission point. This effect was confirmed with SIMION simulations and is visible because of the extended gate of the MCP detector.[36] The slow electron loss shows that electrons are still "boiling off" the vibrationally-hot $[C_7H_9–CO_2]^-$ over the gate timescale, which is consistent with the assignment that the low eKE feature in the photoelectron spectra is a result of thermionic emission (statistical electron ejection) from the anion ground electronic state.[15,20,28,29] Thus, the main product channel following interaction of $[C_7H_9–CO_2]^-$ at $hv = 4.13$ eV or $hv = 4.66$ eV is recovery of the ground electronic state, showing that resonances must be excited at both energies.

In addition to the photoelectron signal in the velocity-map image in Figure 2(c), there is signal arising from dissociated H^- impacting the MCP detector. The offset of the centre of the H^- image relative to the photoelectron image provides a velocity calibration for the kinetic energy release distribution of H^-. Specifically, the velocity vector of H^-, v, is the same as that of the original $[C_7H_9–CO_2]^-$ beam, determined to be $|v| \sim 4.8 \times 10^4$ m s^{-1} from its time-of-flight. This velocity is proportional to the offset in camera pixels of the photoelectron

image centre and the H⁻ image centre (assuming that the photoelectron centre is the true zero-velocity centre of the spectrometer). To analyse the H⁻ fragment, the image was re-centered onto the H⁻ photodetachment feature, reconstructed using polar-onion peeling, and calibrated to yield the kinetic energy release spectrum in Figure 2(d). The H⁻ kinetic energy release exhibits a broad and unstructured peak that closely resembles a Boltzmann distribution (dashed line in Figure 2). The tendency away from the Boltzmann curve at higher kinetic energy is due to the overlap with the electron signal from the parent ion beam. Additionally, as shown in Figure 2(c), the angular distribution of the H⁻ fragment is isotropic. In summary, the Boltzmann-like and isotropic kinetic energy distribution of H⁻ suggest a statistical ground-electronic state dissociation process.

The electronic structure calculations identified two optically-active π^*-resonances, summarized in Figure 3, that are accessible in our experiments. The first resonance at ~4.2 eV (oscillator strength ~0.2) involves charge-transfer of a p-orbital localized on the CO_2 group to π^* orbitals on the polyene. The second resonance at ~4.5 eV (oscillator strength ~1.0) involves $\pi^* \leftarrow \pi$ transitions on the polyene.
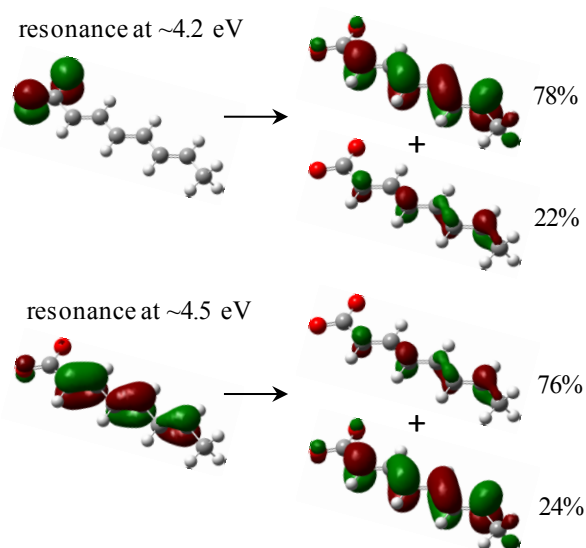

Figure 3: Orbitals involved in the two optically-accessible π^*-resonances

Direct photodetachment from $[C_7H_9-CO_2]^-$ can be identified in Figure 1 by the features extending to 1.4 eV or 1.9 eV in the $hv = 4.13$ eV and $hv = 4.66$ eV spectra, respectively. By extrapolating the high-eKE edge of this feature, the adiabatic binding energy of $[C_7H_9-CO_2]^-$ was determined to be 2.6 ± 0.1 eV. The direct photodetachment peak at both $hv = 4.13$ eV and 4.66 eV is small compared with thermionic emission, suggesting that ground state recovery is very efficient. Indeed, our calculations support that $\pi*$ resonances are photoexcited at both photon energies, so, similar to other aromatic anions,[15,20] there must be efficient internal conversion to the electronic ground state. The velocity-map imaging supports that H^- formation occurs through a ground electronic state dissociation process. However, such a mechanism is inconsistent with the fact that H^- loss is only observed at $hv = 4.13$ eV and not at $hv = 4.66$ eV, suggesting there must be a specific photoexcitation and excited state process (i.e. two-step mechanism) that leads to the observed differences.

Additional insight can be gained by considering the photoelectron feature indicated by the asterisk in Figure 1(a), which extends up to eKE ~ 2.9 eV. Based on the 1.27 ± 0.03 eV electron affinity of the heptatriene, C_7H_9, determined by Brauman and coworkers,[37] this feature can be assigned to direct photodetachment of $[C_7H_9]^-$ by a second (sequential) photon from the ~5 ns laser pulse. Thus, the $hv = 4.13$ eV spectrum indicates that CO_2 is lost very rapidly following excitation of $[C_7H_9-CO_2]^-$. A similar $[C_7H_9]^-$ photodetachment feature is not observed at $hv = 4.66$ eV, suggesting that CO_2 is not dissociated (or to a much lesser extent) at this wavelength. Generally, the loss of CO_2 has been shown to be facile in deprotonated carboxylic acids from a range of collision-induced dissociation and mass spectrometry studies.[38-43] However, these studies only characterise ground state CO_2 loss. In contrast, our photo-initiated experiments show a wavelength-dependent CO_2 loss, which is a typical signature of an excited state process. Finally, it is worth noting that the direct

photodetachment (plus prompt autodetachment)[15,19] channel at $hv = 4.66$ eV is larger than that at $hv = 4.13$ eV, supporting different branching ratios between internal conversion and direct photodetachment (or prompt autodetachment), which is consistent with two different resonances being excited at 4.13 eV and 4.66 eV.

Taking all data together, the consistent mechanistic interpretation is the two-step reaction summarised in Figure 4. First, photoexcitation of the $[C_7H_9–CO_2]^-$ resonance at ~4.2 eV, initiates charge-transfer from the CO_2 group to the polyene chain. There is an associated weakening of the $C_7H_9–CO_2$ bond, which probably induces loss of CO_2 on an excited state potential energy surface to form ground state $[C_7H_9]^-$. Our calculations predict this process would produce $[C_7H_9]^-$ with ~1.9 eV of internal energy. A second photon in the same laser pulse can probe $[C_7H_9]^-$. In contrast, the $[C_7H_9–CO_2]^-$ resonance at ~4.5 eV that is photoexcited at $hv = 4.66$ eV is much brighter and involves a $\pi^* \leftarrow \pi$ transition, but does not involve excitation character that would promote excited state dissociation of CO_2. Hence, $[C_7H_9]^-$ is not formed directly from the 4.5 eV resonance and thermionic emission occurs solely from the parent ground state. In the second mechanismic step, the vibrationally-hot but ground electronic state $[C_7H_9]^-$ produced after 4.13 eV excitation can undergo an intramolecular rearrangement to ultimately dissociate H^-. We propose that the most likely mechanism of such a rearrangement will involve a cyclization reaction to form toluene + H^- due to the high stability of toluene. Such a cyclization would require a series of *trans* to *cis* isomerizations about the double bonds; the first of which may be initiated on the excited state surface,[44] or thermally on the ground state. Isomerization transition state barriers in polyene chains are typically 0.3-1.3 eV[48] in the ground electronic state or can be much smaller in excited electronic states,[45,46,47] implying that several *trans-cis* isomerizations would be available with the thermal energy of $[C_7H_9]^-$. We calculate the asymptotic ΔE for the cyclization reaction to be –0.40 eV (–39 kJ mol^{-1}), i.e. exothermic, supporting that the

cyclization reaction is thermally accessible (assuming that the transition state barrier is less than the total vibrational energy). However, we note that a second photon could also be absorbed by $[C_7H_9]^-$ to photochemically promote cyclization. Experimental studies on similar conjugated molecules and polyenes have shown gas-phase intramolecular cyclization reactions can commonly yield toluene,[10,12,49-51] although it is noteworthy that the present system represents one of the smallest polyenes to yield toluene. Unfortunately, because toluene is neutral, it is difficult to use conventional mass spectrometry methods for characterization, although ion mobility spectrometry may prove useful to characterise the $[C_7H_9]^-$ intermediate species and its isomer distribution.

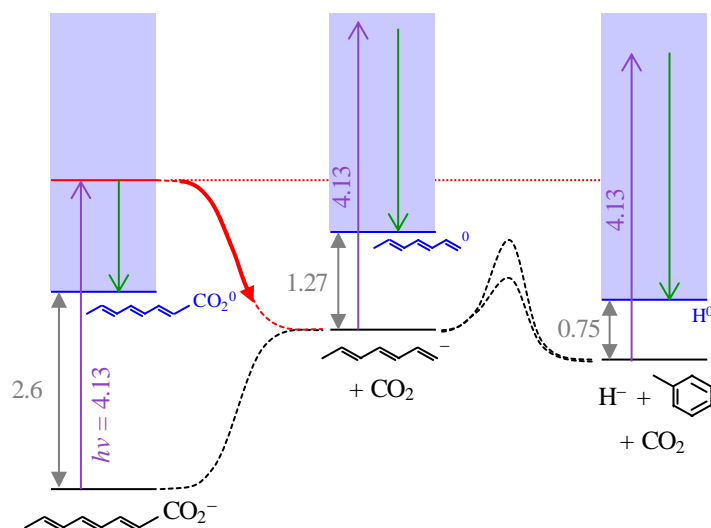Figure 4: Schematic energy level diagram for the production of H^- from $hv = 4.13$ eV photoexcitation of $[C_7H_9–CO_2]^-$. Initial excitation populates a resonance (red) and dissociates to yield $[C_7H_9]^- + CO_2$. The $[C_7H_9]^-$ species can be probed by a second 4.13 eV photon or isomerize to yield toluene and H^-. The H^- can also be detached by a second 4.13 eV photon. The downward arrows (green) indicate the emitted photoelectron energies and the dash-dot line (red) indicates the total energy. All energies are given in eV.

In summary, we have shown that a rich interplay of dynamics can occur in the detachment continuum of large aromatic anions.[15,20] The present study has extended the

current understanding to demonstrate that the dynamics of resonances can induce specific dissociation processes, and therefore facilitate wavelength-specific photochemistry. In $[C_7H_9–CO_2]^-$, specific resonance dynamics induce rapid decarboxylation, which subsequently leads to a intramolecular reaction of the $[C_7H_9]^-$ product. Our work provides the first evidence of a photo-induced cyclization reaction in an anionic polyene and highlights the utility of photoelectron and fragment imaging to probe photochemical reaction intermediates and final products.

Methodology

The experimental set-up has been described in detail elsewhere,[23] and only a brief overview with details specific to the present work follows. The gaseous ion $[C_7H_9–CO_2]^-$ (Figure 1) was generated by electrospray ionisation of ~1 mM solutions of $[C_7H_9–CO_2H]$ (Sigma-Aldrich) dissolved in methanol with a small amount of ammonia to aid deprotonation. Gaseous ions entered a vacuum system through a capillary and were guided into a ring-electrode ion trap. The trapped ions were thermalized and injected into a Wiley-Maclaren time-of-flight mass spectrometer with a 10 Hz repetition rate. The focus of the mass-spectrometer coincided with the centre of a perpendicular velocity-map imaging (VMI) spectrometer.[24] Mass-selected ion packets were intersected with laser pulses (~5 ns duration) from a Nd:YAG pumped OPO operating at 4.13 eV (300 nm) or 4.66 eV (266 nm). The VMI spectrometer is usually operated as a photoelectron spectrometer, where the photoelectrons impact on a gated (100 ns) multichannel plate (MCP) detector coupled to a phosphor screen. The resulting events are digitally captured using a CCD camera. For photoelectron spectroscopy, the parent ion beam energy has only a small influence on the electron trajectories because of the very large mass difference between the parent ion and photoelectrons. VMI images were reconstructed using the polar-onion peeling algorithm and

photoelectron spectra were calibrated using the photoelectron spectrum of I^-.[25] The resolution of the photoelectron spectra is ~5%.

Supporting electronic structure calculations were performed with Gaussian 09 and GAMESS-US.[52,53] First, CAM-B3LYP//aug-cc-pVTZ calculations were performed to determine equilibrium geometries and G4 theory was used to compute thermochemical properties.[26,54,55] Calculation of resonance energies for $[C_7H_9–CO_2]^-$ was performed at the multistate XCMQDPT2 level of theory using the aug-cc-pVDZ basis set excluding the most diffuse set of d functions on carbon atoms for computational tractability.[27,55] The CASSCF reference wavefunction used 10 electrons in 13 orbitals, which constituted the most important p, π, and π^* orbitals from a preliminary CIS calculation. This level of theory has previously proven reliable to determine resonance energetics in a range of conjugated and aromatic anions.[14,15,17,20,31]

References

(1)   Delgado-Vargas, F.; Jiménez, A. R.; Paredes-López, O. Natural Pigments: Carotenoids, Anthocyanins, and Betalains - Characteristics, Biosynthesis, Processing, and Stability. *Crit. Rev. Food Sci. Nut.* **2000**, 40, 173-289.

(2)   Hudson, B.; Kohler, B. Linear Polyene Electronic Structure and Spectroscopy. *Annu. Rev. Phys. Chem.* **1974**, 25, 437-460.

(3)   Siefermann-Harms, D. Carotenoids in Photosynthesis. I. Location in Photosynthetic Membranes and Light-Harvesting Function. *Biochim. Biophys. Acta* **1985**, 811, 325-355.

(4)   Young, A. J., Britton, G., Eds. Carotenoids in Photosynthesis; Springer: Dordrecht, Netherlands, 1993.

(5)   Birge, R. R. Photophysics and Molecular Electronic Applications of the Rhodopsins. *Annu. Rev. Phys. Chem.* **1990**, 41, 683-733.

(6)   Yoshizawa, T.; Wald, G. Pre-Lumirhodopsin and the Bleaching of Visual Pigments. *Nature* **1963**, 197, 1279-1286.

(7)   Schoenlein, R. W.; Peteanu, L. A.; Mathies, R. A.; Shank, C. V. The First Step in Vision: Femtosecond Isomerization of Rhodopsin. *Science* **1991**, 254, 412-415.

(8)   Polli, D.; Altoè, P.; Weingart, O.; Spillane, K. M.; Manzoni, C.; Brida, D.; Tomasello, G.; Orlandi, G.; Kukura, P.; Mathies, R. A.; Garavelli, M.; Cerullo, G. Conical Intersection Dynamics of the Primary Photoisomerization Event in Vision. *Nature* **2010**, 467, 440-443.

(9)   Toker, Y.; Rahbek, D. B.; Kiefer, H. V.; Rajput, J.; Antoine, R.; Dugourd, P.; Nielsen, S. B.; Bochenkova, A. V.; Andersen, L. H. Photoresponse of the Protonated Schiff-Base Retinal Chromophore in the Gas Phase. *Phys. Chem. Chem. Phys.* **2013**, 15, 19566-19569.

(10)   Coughlan, N. J. A.; Catani, K. J.; Adamson, B. D.; Wille, U.; Bieske, E. J. Photoisomerization Action Spectrum of Retinal Protonated Schiff Base in the Gas Phase. *J. Chem. Phys.* **2014**, 140, 164307.

(11)   Musbat, L.; Nihamkin, M.; Ytzhak, S.; Hirshfeld, A.; Friedman, N.; Dilger, J. M.; Sheves, M.; Toker, Y. Isotope Labeling Study of Retinal Chromophore Fragmentation. *J. Phys. Chem. A* **2016**, 120, 2547-2549.

(12)   Coughlan, N. J. A.; Adamson, B. D.; Catani, K. J.; Wille, U.; Bieske, E. J. Ion Mobility Unlocks the Photofragmentation Mechanism of Retinal Protonated Schiff Base. *J. Phys. Chem. Lett.* **2014**, 5, 3195-3199.

(13)   van Breemen, R. B.; Dong, L.; Pajkovic, N. D. Atmospheric Pressure Chemical Ionization Tandem Mass Spectrometry of Carotenoids. *Int. J. Mass Spectrom.* **2012**, 312, 163-172.

(14)   West, C. W.; Bull, J. N.; Antonkov, E.; Verlet, J. R. R. Anion Resonances of para-Benzoquinone Probed by Frequency-Resolved Photoelectron Imaging. *J. Phys. Chem. A* **2014**, 118, 11346-11354.

(15)   Bull, J. N.; West, C. W.; Verlet, J. R. R. On the Formation of Anions: Frequency-, Angle-, and Time-Resolved Photoelectron Imaging of the Menadione Radical Anion. *Chem. Sci.* **2015**, 6, 1578-1589.

(16)   West, C. W.; Bull, J. N.; Hudson, A. S.; Cobb, S. L.; Verlet, J. R. R. Excited State Dynamics of the Isolated Green Fluorescent Protein Chromophore Anion Following UV Excitation. *J. Phys. Chem. B* **2015**, 119, 3982-3987.

(17)   Bull, J. N.; West, C. W.; Verlet, J. R. R. Anion Resonances and Above-Threshold Dynamics of Coenzyme Q_0. *Phys. Chem. Chem. Phys.* **2015**, 17, 16125-16135.

(18)   Horke, D. A.; Li, Q.; Blancafort, L.; Verlet, J. R. R. Ultrafast Above-threshold Dynamics of the Radical Anion of a Prototypical Quinone Electron-Acceptor. *Nat. Chem.* **2013**, 5, 711-717.

(19)   Anstöter, C. S.; Bull, J. N.; Verlet, J. R. R. Ultrafast Dynamics of Temporary Anions Probed Through the Prism of Photodetachment. *Int. Rev. Phys. Chem.* **2016**, 35, 509-538.

(20)   Bull, J. N.; West, C. W.; Verlet, J. R. R. Internal Conversion Outcompetes Autodetachment From Resonances in the Deprotonated Tetracene Anion Continuum. *Phys. Chem. Chem. Phys.* **2015**, 17, 32464-32471.

(21)   Davis, A. V.; Wester, R.; Bragg, A. E.; Neumark, D. M. Time-Resolved Photoelectron Imaging of the Photodissociation of I_2^-. *J. Chem. Phys.* **2003**, 118, 999-1002.

(22)   Baer, T.; Hase, W. L. Unimolecular Reaction Dynamics: Theory and Experiments; Oxford University Press: Oxford, UK; 1996.

(23)   Lecointre, J.; Roberts, G. M.; Horke, D. A.; Verlet, J. R. R. Ultrafast Relaxation Dynamics Observed Through Time-Resolved Photoelectron Angular Distributions. *J. Phys. Chem. A* **2010**, 114, 11216-11224.

(24)   Horke, D. A.; Roberts, G. M.; Lecointre, J.; Verlet, J. R. R. Velocity-Map Imaging at Low Extraction Fields. *Rev. Sci. Instrum.* **2012**, 83, 063101.

(25)   Roberts, G. M.; Nixon, J. L.; Lecoitre, J.; Wrede, E.; Verlet, J. R. R. Toward Real-Time Charged-Particle Image Reconstruction Using Polar Onion Peeling. *Rev. Sci. Instrum.* **2009**, 80, 053104.

(26)   Curtiss, L. A.; Redfern, P. C.; Raghavachari, K. Gaussian-4 Theory. *J. Chem. Phys.* 2007, 126, 084108.

(27)   Granovsky, A. A. Extended Multi-Configuration Quasi-Degenerate Perturbation Theory: The New Approach to Multi-State Multi-Reference Perturbation Theory. *J. Chem. Phys.* **2011**, 134, 214113.

(28)   Andersen, J. U.; Bonderup, E.; Hansen, K. Thermionic Emission from Clusters. *J. Phys. B: At. Mol. Opt. Phys.* **2002**, 35, R1.

(29)   Campbell, E. E.; Levine, R. D. Delayed Ionization and Fragmentation en route to

Thermionic Emission: Statistics and Dynamics. *Annu. Rev. Phys. Chem.* **2000**, 51, 65-98.

(30)   Zare, R. N. Photoejection Dynamics. *Mol. Photochem.* **1972**, 4, 1-37.

(31)   Bull, J. N.; West, C. W.; Verlet, J. R. R. Ultrafast Dynamics of Formation and

Autodetachment of a Dipole-Bound State in an Open-Shell π-Stacked Dimer Anion. *Chem.

Sci.* **2016**, 7, 5352-5361.

(32)   Jordan, K. D.; Wang, F. Theory of Dipole-Bound Anions. *Annu. Rev. Phys. Chem.*

2003, 54, 367-396.

(33)   Shiell, R. C.; Hu, X. K.; Hu, Q. C. J.; Hepburn, J. W. Threshold Ion-Pair Production

Spectroscopy (TIPPS) of H_2 and D_2. *Faraday Discuss.* **2000**, 115-343, 331.

(34)   Brenton, A. G.; Morgan, R. P.; Beynon, J. H. Unimolecular Ion Decomposition.

Annu. Rev. Phys. Chem. **1979**, 30, 51-78.

(35)   Ashfold, M. N. R.; King, G. A.; Nix, M. G. D.; Oliver, T. A. A. High-Resolution

Photofragment Translational Spectroscopy Using Rydberg Tagging Methods. In Handbook of

High-resolution Spectroscopy; John Wiley & Sons, Ltd, 2011.

(36)   Dahl, D. A. SIMION for the Personal Computer in Reflection. *Int. J. Mass. Spectrom.*

2000, 200, 3-25.

(37)   Zimmerman, A. H.; Gygax, R.; Brauman, J. I. Electron Photodetachment

Spectroscopy of Polyene Anions. Electron Affinities of Pentadienyl and Heptatrienyl

Radicals. *J. Am. Chem. Soc.* **1978**, 100, 5595-5597.

(38)   Segura, P.; Bunnett, J. F.; Villanova, L. Substituent Effects on the Decarboxylation of Dinitrobenzoate Ions. Representative Aromatic SE1 Reactions. *J. Org. Chem.* **1985**, 50, 1041-1045.

(39)   Karas, M.; Bachmann, D.; Hillenkamp, F. Influence of the Wavelength in High-Irradiance Ultraviolet Laser Desorption Mass Spectrometry of Organic Molecules. *Anal. Chem.* **1985**, 57, 2935-2939.

(40)   Graul, S. T.; Squires, R. R. The Existence of Alkyl Carbanions in the Gas Phase. *J. Am. Chem. Soc.* **1988**, 110, 607-608.

(41)   Bowie, J. H. The Fragmentations of Even-Electron Organic Negative Ions. *Mass Spectrom. Rev.* **1990**, 9, 349-379.

(42)   Squires, R. R. Gas-Phase Carbanion Chemistry. *Acc. Chem. Res.* **1992**, 25, 461-467.

(43)   Gronert, S. Mass Spectrometric Studies of Organic Ion/Molecule Reactions. *Chem. Rev.* **2001**, 101, 329-360.

(44)   Levine, B. G.; Martínez, T. J. Isomerization Through Conical Intersections. *Annu. Rev. Phys. Chem.* **2007**, 58, 613-634.

(45)   Dugave, C.; Demange, L. Cis−Trans Isomerization of Organic Molecules and Biomolecules: Implications and Applications. *Chem. Rev.* **2003**, 103, 2475-2532.

(46)   Send, R.; Sundholm, D.; Johansson, M. P.; Pawłowski, F. Excited State Potential Energy Surfaces of Polyenes and Protonated Schiff Bases. *J. Chem. Theory Comput.* **2009**, 5, 2401-2414.

(47)   Lee, H. M.; Kim, J.; Kim, C.-J.; Kim, K. S. Ab initio Study of the Isomerization of Retinal Chromophore and its Derivatives. *J. Chem. Phys.* **2002**, 116, 6549-6559.

(48)   Dilger, J.; Musbat, L.; Sheves, M.; Bochenkova, A. V.; Clemmer, D. E.; Toker, Y. Direct Measurement of the Isomerization Barrier of the Isolated Retinal Chromophore. *Angew. Chem. Int. Ed.* **2015**, 54, 4748-4752.

(49)   Guaratini, T.; Lopes, N. P.; Pinto, E.; Colepicolo, P.; Gates, P. J. Mechanism for the Elimination of Aromatic Molecules From Polyenes in Tandem Mass Spectrometry. *Chem. Comm.* **2006**, 4110-4112.

(50)   Onyewu, P. N.; Daun, H.; Ho, C. T. Formation of Two Thermal Degradation Products of β-carotene. *J. Agric. Food Chem.* **1982**, 30, 1147-1151.

(51)   Kuck, D.; Mormann, M. Mass Spectrometry and Gas-Phase Ion Chemistry of Dienes and Polyenes. In The Chemistry of Dienes and Polyenes, vol. 2; John Wiley & Sons, Ltd.; 2009.

(52)   Frisch, M. J.; Trucks, G. W.; Schlegel, H. B.; Scuseria, G. E.; Robb, M. A.; Cheeseman, J. R.; Scalmani, G.; Barone, V.; Mennucci, B.; Petersson, G. A.; *et al.* Gaussian 09, Gaussian, Inc. Wallingford CT, 2009.

(53)   Schmidt, M. W.; Baldridge, K. K.; Boatz, J. A.; Elbert, S. T.; Gordon, M. S.; Jensen, J. H.; Koseki, S.; Matsunaga, N.; Nguyen, K. A.; Su, S.; Windus, T. L.; Dupuis, M.; Montgomery, J. A. General Atomic and Molecular Electronic Structure System. *J. Comput. Chem.* **1993**, 14, 1347-1363.

(54)   Yanai, T.; Tew, D. P.; Handy, N. C. A New Hybrid Exchange–Correlation Functional Using the Coulomb-Attenuating Method (CAM-B3LYP). *Chem. Phys. Lett.* **2004**, 393, 51-57.

(55)   Dunning Jr., T. H. Gaussian Basis Sets for use in Correlated Molecular Calculations. I. The Atoms Boron Through Neon and Hydrogen. *J. Chem. Phys.* **1989**, 90, 1007.